Heat transport in a convecting layer heated from within and below

William B. Moore[1]

Received 29 September 2006; revised 15 August 2008; accepted 9 September 2008; published 18 November 2008.

[1] The heat transport scaling relationships for fluids heated from within and below are established based on numerical calculations of isoviscous Boussinesq convection at infinite Prandtl number. The internal temperatures scale in a way that is similar to the internally heated case but with an offset equal to the average of the two boundary temperatures, reflecting the underlying temperature structure of bottom-heated convection. The heat fluxes through the boundaries scale as a linear combination of the end-member modes of heat transport, consistent with the effects of internal heating on the interior temperature. The boundary layer thicknesses, however, depend on H and Ra in a nonintuitive way. As the internal temperature increases with the addition of internal heating, the upper thermal boundary layer thickens despite the increased temperature drop across the layer (the reverse is true for the bottom boundary layer). This is inconsistent with the idea that the boundary layer thickness is controlled by a stability condition on the local Rayleigh number, which would predict that the boundary layer would thin as the temperature drop increases. Deriving boundary layer thicknesses from the scalings for heat flux and boundary layer temperature drop provides an excellent fit to the model results and reveals the importance of plumes arriving from the other boundary layer in establishing the boundary layer thickness. This suggests that, although widely used, boundary layer stability analysis is not an accurate description of the processes controlling boundary layer thickness in systems with two active boundary layers at moderate Ra.

Citation: Moore, W. B. (2008), Heat transport in a convecting layer heated from within and below, *J. Geophys. Res.*, *113*, B11407, doi:10.1029/2006JB004778.

1. Introduction

[2] Convecting planetary mantles transport heat from below, as well as heat generated within them. About 10% of the heat flow at the surface of the Earth, for example, is thought to come from the core, driving the geodynamo [*Davies*, 1999]. Europa's floating ice shell is another example, where tidal heating contributes both an internal and a basal heat source (from heating in deeper layers). This situation is known as mixed-mode heating, and it is common in terrestrial planet mantles as well as the silicate mantles and floating ice shells of the outer-planet satellites.

[3] Despite the ubiquity of mixed-mode heating, planetary thermal modeling to date has typically employed end-member parameterizations with internal or bottom heating only [e.g., *Hauck and Phillips*, 2002; *Hauck et al.*, 2004; *Reese et al.*, 1999]. These parameterizations have become quite sophisticated, accounting for complex rheologies and spherical-shell geometry [*Reese et al.*, 2005], but attempts to model mixed-mode heating have been few [*Sotin and Labrosse*, 1999], and did not provide a scaling for the structure of the bottom boundary layer or the heat flow through the base as a function of the convective parameters. Internal heating modifies the interior temperature of a convecting layer. This provides a feedback, through temperature-dependent viscosity, that acts as a thermostat regulating the interior temperature of planets [*Tozer*, 1967]. In situations where tidal dissipation is an important heat source (Jupiter's moon Io, for example), the internal temperature also controls the rate of heating through the dependence of heat production on viscosity, providing a further feedback. Modeling the thermal evolution of such systems requires accurate parameterizations of the temperature structure and the heat fluxes within the layer.

[4] Internal heating has a significant effect beyond simply increasing the internal temperature of the layer. By breaking the symmetry between the upper and lower boundary layers, internal heating leads to changes in boundary layer thickness which are opposite to that predicted by the changing boundary layer stability (as measured by the boundary layer Rayleigh number). This reveals that there is a different process governing heat transport through the boundary layer in the range of Rayleigh numbers where most planetary mantles and ice shells are found (10^5–10^8). It is shown here that convective heat transport in this range of Ra is between two asymptotic regimes, one dominated by thermal boundary layer instability at high Ra ($\geq 10^9$) and one dominated by the arrival of plumes from the opposite layer at low Ra, and that no single scaling applies. This is a significant departure from existing theory and the implications for

[1]Institute of Geophysics and Space Physics and Department of Earth and Space Sciences, University of California, Los Angeles, Los Angeles, California, USA.

0148-0227/08/2006JB004778$09.00

planetary thermal history modeling, as well as our understanding of how planets work are profound.

[5] This paper presents two-dimensional numerical calculations of convection in an isoviscous layer heated from below and within which are used to derive scalings for the mean internal temperature, internal temperature gradient, boundary layer thicknesses, and basal and surface heat fluxes as a function of the convective parameters (expressed through the internal heating rate and the Rayleigh number). Isoviscous models are chosen to isolate the effect of mixed-mode heating from that of temperature-dependent viscosity. It has been shown that, for the large temperature dependence characteristic of planetary materials (ice and rock), the convection is essentially isoviscous beneath a stagnant, conductive lid [*Grasset and Parmentier*, 1998; *Reese et al.*, 1999; *Solomatov and Moresi*, 2000]. The extension to temperature-dependent viscosity will be dealt with in a future paper. The range of Rayleigh numbers chosen for this study ($10^4 < Ra < 10^8$) covers the expected *effective* Rayleigh numbers governing the actively convecting layer beneath the stagnant lids of most planetary bodies.

[6] The numerical model is detailed in the next section, followed by the development of scaling relationships for mixed-mode convection. These relationships are discussed in the final section. The key to understanding the behavior of mixed-mode convection is to recognize that the basic state (zero heating) is different when the bottom boundary temperature is held constant than in the usual situation where the bottom heat flux is set to zero. When the appropriate reference temperature is used, the familiar scalings reappear in the mixed-heating case.

2. Numerical Model

[7] The numerical experiments are performed in a 4×1 or 8×1, two-dimensional domain with reflecting side boundaries, constant temperature upper and lower boundaries and varying amounts of internal heating. Within this domain the equations of mass, momentum, and energy conservation in an infinite Prandtl number, Boussinesq fluid are solved numerically by finite volume discretization on a staggered grid using STAG3D [*Tackley*, 1996]. For the isoviscous cases considered here, there are two controlling parameters. The temperature is non-dimensionalized by the temperature difference between the top and bottom of the layer ΔT^*, leading to the standard bottom-heating definition of the Rayleigh number Ra:

$$Ra = \frac{\rho g \alpha \Delta T^* D^3}{\eta \kappa} \tag{1}$$

where ρ is the density, g is the acceleration of gravity, α is the thermal expansivity, D is the thickness of the layer, η is the viscosity and κ the thermal diffusivity. As this study is intended to be quite general, specific values for these quantities will not be adopted.

[8] The specific internal heating rate H^* (W/kg) defines a second dimensionless temperature scale ΔT_H

$$\Delta T_H = \frac{\rho H^* D^2}{k} \tag{2}$$

where k is the thermal conductivity, and the asterisk indicates a dimensional quantity. Although a Rayleigh number based on this temperature scale (Ra_H) is typically defined for internally heated convection, to avoid confusion between two different Rayleigh numbers the dimensionless heating rate H given by

$$H = \frac{\rho H^* D^2}{k \Delta T^*}, \tag{3}$$

which is equal to Ra_H/Ra is used instead [*Schubert et al.*, 2001]. For the remainder of this report, the dimensionless temperature difference ΔT and layer depth D are set to 1, and non-dimensional quantities will be used. All constant non-dimensional material parameters (e.g., D, ρ, k) will be given the value 1. A range of Ra from 10^4 to 10^8 and H up to 10^2 was explored to quantitatively determine the dependence of heat transport through the boundaries and the internal temperature distribution on the controlling parameters.

[9] The time evolution of the system uses the MPDATA scheme of *Smolarkiewicz* [1984], and the time step is limited by the Courant condition. The calculations presented here use a 256×64 grid at $Ra < 10^7$, and twice that resolution for the higher Ra cases. All cases were run to statistical steady state, and then at least an equal amount of time beyond. Properties were time averaged over this period. Certain low-Ra cases require wider domains than 4×1 because these weakly convecting cases have steady or nearly-steady solutions with fixed aspect-ratio cells. If an integer number of the steady cells is not compatible with the fixed-width domain, spurious time-dependence is introduced as the number of cells oscillates about the preferred non-integer value. This affects the Nusselt numbers and the mean temperature [*Grigne et al.*, 2005]. An 8×1 domain (and in two cases a 16×1 domain was tested) is used when such quasi-steady behavior is observed, which reduces the problem.

3. Results

[10] For thermal history calculations, the heat flow through the boundaries of the layer is required as a function of the convective parameters Ra and H. The heat flow out of the top of the layer is typically represented by the Nusselt number Nu_{top}

$$Nu_{top} = \left.\frac{dT}{dz}\right|_{z=1} = H + Nu_{bot} = H + \left.\frac{dT}{dz}\right|_{z=0} \tag{4}$$

where Nu_{bot} is the non-dimensional bottom boundary heat flux. An approximation to the horizontally averaged temperature profile in the layer is also necessary for the purposes of comparing with observations and, in cases where tidal heating may be important, for calculating the viscosity-dependent heating.

[11] First, we review the end-member heating cases (for a thorough discussion see *Schubert et al.* [2001]). Figure 1 shows the horizontally and time-averaged temperature profiles of three calculations at $Ra = 10^5$: bottom-heated ($H = 0$), internally heated ($H = 10$), and mixed heating ($H = 10$).

[12] A layer heated from below by maintenance of a fixed temperature difference between the upper and lower bound-

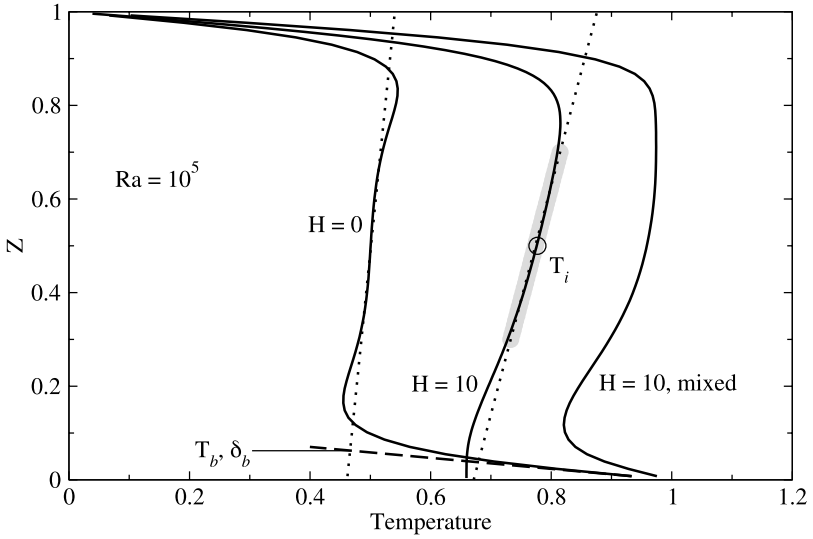

Figure 1. Horizontally and time-averaged temperature for three cases with $Ra = 10^5$: bottom-heated ($H = 0$), internally heated ($H = 10$), and mixed heating ($H = 10$, mixed). The interior temperature and gradient are determined from a linear fit (dotted) over the gray region ($0.3 \leq z \leq 0.7$). The boundary layer properties are determined from the intersection of this line, with the gradient extrapolated from each surface (dashed), as shown for the bottom-heated case.

aries results in a temperature structure with two boundary layers separated by an isothermal (or adiabatic if the material is compressible) core. The temperature in the core is the average of the two boundary temperatures, and the temperature drop across each boundary layer is half the total. As convective vigor increases, the boundary layers must thin in order to carry more heat, since the temperature drop is fixed. At equilibrium, the two layers must transport the same amount of heat and therefore have the same average thickness. This thickness is determined by the criterion for convective stability of the boundary layer, that is, the boundary layer will thicken until the Rayleigh number (calculated for the boundary layer alone) exceeds a critical value and it becomes unstable and detaches. The (non-dimensional) critical boundary layer thickness δ scales with the Rayleigh number according to: $\delta \sim Ra^{-1/3}$, thus the heat flow through each boundary scales as: $Nu \sim Ra^{1/3}$.

[13] A layer heated from within with no heat flux from below has only a single boundary layer at the top. At equilibrium, this boundary layer must carry all of the heat generated in the layer (proportional to H). The boundary layer thickness is controlled by the stability criterion as above, so the interior temperature adjusts until the heat production is balanced by heat flow across the layer. The resulting temperature difference across the boundary layer scales as $Ra^{-1/4}H^{3/4}$ (or $Ra_H^{-1/4}\ H$). When this temperature drop is factored into the stability criterion for the boundary layer, the boundary layer thickness is found to scale as $(RaH)^{-1/4}$.

[14] Here we seek a parameterization for the heat flow and temperature structure within a layer with mixed heating. The results of 49 two-dimensional calculations are summarized in Table 1. The heat flow at the boundaries is directly computed from the output temperature field. The temperature structure is computed from horizontal and time averages of the temperature field. We divide the domain into two (often unequal) boundary layers and a typically subadiabatic interior. The parameterizations are all derived from linear regressions to the data in table datatable. Rather than report formal errors on the coefficients, which are not very meaningful in the absence of good error estimates for the measured quantities, the average fractional misfits, calculated as $\langle$(measured - model)/model$\rangle$, will be reported. All derived parameter values will be given to out to the most significant digit of the formal error.

[15] There are two typical ways to approach defining the thermal boundary layers. The first is to treat the boundary layer as a region in which the process of conduction dominates and to consider the transient growth of the conductive boundary layer toward instability. The second, simpler approach is to consider the layer as a region across which a steady heat flow is conducted. In both cases the heat flow is inversely proportional to the boundary layer thickness. The difference is that the actual temperature structure of the boundary layer is more closely approximated by a transient, rather than a steady conduction profile, as is evident from the curvature of the temperature profiles in Figure 1. For developing a simple parameterization for use in thermal history modeling, however, the steady-state boundary layer is sufficient.

4. Interior Temperature

[16] As mentioned above and discussed in more detail below, the interior temperature is not constant with height in the presence of internal heating, rather, the interior is subadiabatic. We parameterize the temperature in the interior using a linear fit to the horizontally and time-averaged profile over the vertical interval between 0.3 and 0.7 dimensionless height (shown in gray in Figure 1). This fit is used to specify the interior temperature T_i, which is the value of the fit at mid-depth, and the interior temperature gradient. The

Table 1. Convection Simulation Results

Ra	H	Nu_{bot}	δ_{bot}	T_{bot}	Nu_{top}	δ_{top}	T_{top}	T_i
10^4	0	4.88013	0.115536	0.436171	4.88013	0.115339	0.562869	0.499504
	10^0	4.36535	0.118729	0.481704	6.82451	0.089242	0.609033	0.542998
	3×10^0	2.87828	0.117045	0.663113	5.87802	0.146526	0.861284	0.766165
	10^1	−0.797778	0.263661	1.21034	9.20196	0.166386	1.53108	1.34334
	3×10^1	−7.86706	0.111877	1.88014	22.1058	0.121403	2.68371	2.28692
	10^2	−29.0054	0.119402	4.4633	71.0968	0.0947465	6.73617	5.56408
3×10^4	0	6.88342	0.0778453	0.464158	6.88348	0.0776299	0.534364	0.499252
10^5	0	8.53894	0.0624905	0.466397	8.56196	0.0625618	0.535652	0.501027
	10^0	8.00397	0.0602742	0.517567	9.01151	0.0650723	0.5864	0.552172
	3×10^0	6.69498	0.0598748	0.599139	9.73759	0.0730488	0.711319	0.656081
	10^1	3.11074	0.0428524	0.866697	13.1306	0.0783247	1.02845	0.950838
	3×10^1	−4.17425	0.0727919	1.30385	25.6824	0.0626268	1.60841	1.45434
	10^2	−20.7691	0.0947651	2.96819	79.1309	0.0469224	3.71301	3.31984
3×10^5	0	11.661	0.0438859	0.488247	11.6536	0.0449236	0.523522	0.505905
	10^0	11.1465	0.043266	0.517736	12.1784	0.0456407	0.555831	0.536833
	3×10^0	10.4449	0.0405823	0.576122	13.4344	0.0469146	0.63027	0.603384
	10^1	6.70087	0.0364985	0.755428	16.4309	0.0503325	0.827008	0.79176
	3×10^1	−1.00117	0.0584188	1.05849	26.7924	0.0463915	1.24294	1.14947
	10^2	−14.1295	0.076053	2.07459	66.2982	0.0376619	2.49692	2.27661
10^6	0	16.938	0.0297927	0.495372	16.7821	0.0307597	0.516212	0.505803
	10^0	16.713	0.0283076	0.526896	17.7681	0.0302096	0.536768	0.531842
	3×10^0	16.4312	0.0256868	0.577935	19.4992	0.0303414	0.591633	0.584818
	10^1	11.8951	0.0270186	0.678611	21.9567	0.0330386	0.725419	0.702165
	3×10^1	2.42383	0.0248622	0.939738	32.3851	0.0320493	1.03792	0.989203
	10^2	−13.6364	0.0671144	1.9152	86.2769	0.0256279	2.21109	2.05638
3×10^6	0	27.8117	0.0182509	0.492413	28.0179	0.0176424	0.494303	0.494041
	10^0	24.7895	0.0193116	0.521275	25.9999	0.0202719	0.527068	0.524174
	3×10^0	22.6073	0.0196719	0.555272	25.8736	0.0218362	0.564981	0.560138
	10^1	18.3497	0.0204737	0.624315	28.5259	0.0227519	0.64902	0.636697
	3×10^1	8.59345	0.0209849	0.819668	37.7514	0.0231851	0.875268	0.847532
	10^2	−8.84635	0.0511532	1.45252	80.6629	0.0202552	1.63385	1.54017
10^7	0	33.3108	0.0151875	0.494093	33.3495	0.0150215	0.500959	0.497525
	10^0	32.5224	0.0152322	0.504612	33.7392	0.0151245	0.510288	0.50745
	3×10^0	32.0459	0.0142584	0.543077	34.7455	0.0157506	0.547263	0.545173
	10^1	26.8922	0.0151898	0.591513	36.9556	0.0165672	0.612252	0.601897
	3×10^1	16.3144	0.0157902	0.742393	46.3148	0.0168692	0.781293	0.761865
	10^2	−5.12413	0.038766	1.19864	94.8921	0.0139892	1.32746	1.26137
3×10^7	0	49.4404	0.0103011	0.490711	50.0709	0.00985667	0.493532	0.492121
	10^0	48.2888	0.0102927	0.50298	49.8821	0.0101626	0.50693	0.504954
	3×10^0	48.0705	0.00957881	0.539542	51.6567	0.0105317	0.544034	0.54179
	10^1	42.0235	0.0101165	0.57487	52.6616	0.0110564	0.582247	0.578562
	3×10^1	30.4841	0.0108519	0.66919	60.7095	0.011397	0.691905	0.680554
	10^2	3.77893	0.00520358	0.980336	99.0586	0.0106469	1.05467	1.01771
10^8	0	66.975	0.00751477	0.496698	67.434	0.00742489	0.50069	0.498694
	10^0	65.8306	0.00740138	0.512763	68.1512	0.00756854	0.515805	0.514284
	3×10^0	63.8088	0.00745265	0.524455	68.4807	0.00771879	0.528588	0.526522
	10^1	59.623	0.00741668	0.557795	70.2319	0.0079959	0.561567	0.559682
	3×10^1	47.5037	0.00775871	0.631433	77.6329	0.00828017	0.642813	0.637126
	10^2	15.4059	0.00794346	0.877624	115.377	0.00798007	0.920717	0.899171

steady-state boundary layer thickness and temperature are determined by finding the point at which a constant gradient temperature profile that matches the boundary heat flow (dashed in Figure 1) extended inward from the boundary intersects the interior temperature fit (dotted in Figure 1). It should be remembered that this is an effective boundary layer only, and that this structure is not realized at any point within the domain. For low Ra, when the boundary layer can be quite thick, the fit to the internal gradient can become contaminated by the influence of the boundary layers. All of the parameter fits presented therefore exclude the models with Ra below 10^5, although these models are shown in the plots.

[17] The addition of internal heat to a basally heated layer breaks the symmetry of the boundary layers, since now the upper boundary must transport the heat coming through the bottom as well as the heat produced internally, that is, $Nu_{top} = Nu_{bot} + H$. This extra heat is transported by an increase in the internal temperature which increases the temperature drop across the upper boundary layer, exactly like the purely internally heated case. The difference in the mixed case is that the internal temperature increase caused by internal heating is over and above the bottom-heated temperature profile. Thus, when the internal temperature T_i is referenced to that produced by the bottom-heated case (the mean of the top and bottom temperatures which is 0.5 in non-dimensional values), the typical internally heated scaling is recovered:

$$T_i = 0.49 + 1.24 H^{3/4} Ra^{-1/4} \quad (5)$$

as shown in Figure 2 and compiled in Table 2. The average misfit is less than 2%. Note that only those models in which heat is transported from below ($Nu_{bot} > 0$) are included in these fits, as well as the subsequent fits for the boundary

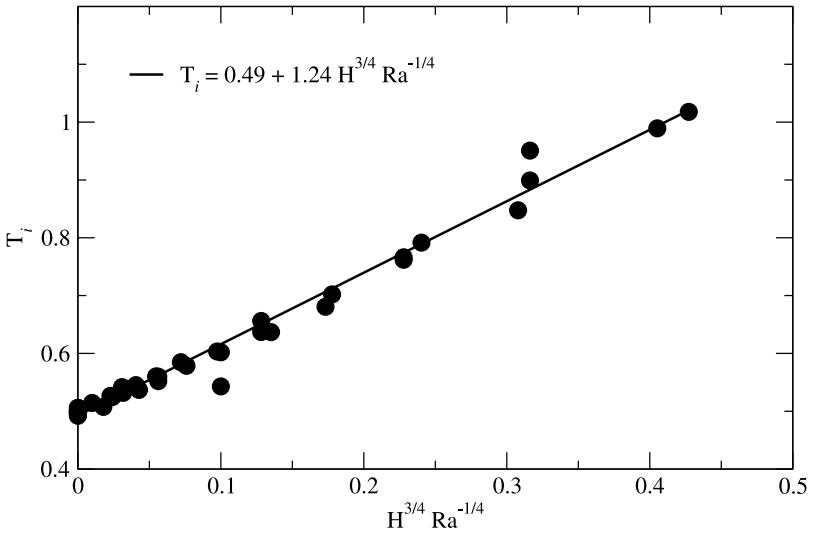

Figure 2. Interior temperature T_i vs. $H^{3/4}Ra^{-1/4}$. The solid line shown is the fitting function which is given in (5).

layer temperature drops. A slightly better fit is found by allowing the exponents to vary from the internally heated scaling, but the difference is small. This scaling is essentially identical to that ($0.5 + 1.236H^{3/4}\ Ra^{-1/4}$) found by *Sotin and Labrosse* [1999] in their study of this problem.

5. Boundary Layer Temperature Drops

[18] The temperature drop across each boundary layer is shown in Figure 3 as a function of $H^{3/4}\ Ra^{-1/4}$. Note the divergence from the symmetrical boundary layers at $H = 0$. The temperature drops scale similarly to the internal temperature, with the upper boundary temperature drop increasing and the lower boundary temperature drop decreasing. The best fit scalings for the upper and lower boundary layer temperature drops are:

$$\Delta T_{top} = 0.499 + 1.33\ H^{3/4}Ra^{-1/4} \tag{6}$$

$$\Delta T_{bot} = 0.514 - 1.13\ H^{3/4}\ Ra^{-1/4} \tag{7}$$

The average misfits are less than 3% for the upper boundary layer and less than 5% for the lower boundary layer. This scaling follows the interior temperature scaling, which shows that the additional heat coming from internal heating is being transported through the boundary layer in the same way it would without there being any heat from below.

[19] The fact that the sum of the top and bottom temperature drops exceeds the total temperature drop across the system (1 in dimensionless units), a discrepancy which increases with H, is due to an aspect of internally heated convection that has not been quantitatively analyzed to date. The interior of an internally heated layer tends to have a subadiabatic gradient, that is, the bottom of the layer is somewhat colder than the top, as shown in Figure 1. The interior gradient is measured from a straight line fit to the averaged temperature profile as described above. This gradient occurs in internally heated fluid layers because the fluid upwells passively in response to detachment of the upper boundary layer. In mixed heating cases, this passive flow balances the excess input to the lower boundary layer from the more active upper layer. As fluid moves upward in the layer, the internal heating is gradually increasing the temperature. The temperature gradient $d\mathrm{T}/dz$ is thus proportional to the heating rate ($d\mathrm{T}/dt$) and inversely proportional to the upwelling velocity (dz/dt). The upwelling velocity scales as $Ra_H^{1/2}$ [*Turcotte and Schubert*, 2001], thus the subadiabatic gradient scales as $Ra_H^{-1/2}H$ or $(H/Ra)^{-1/2}$, as shown in Figure 4. The relationship holds for mixed heating cases as well (although there is more scatter). The best-fit scaling for both mixed and internally heated cases is shown by the solid line and is given by $d\mathrm{T}/dz = 23\ (H/Ra)^{-0.52}$, which is very close to the theoretical scaling. The fit is much better for the purely internally heated cases (12% average misfit) than the mixed heating cases (29% average misfit), suggesting that mixing driven by the passage of hot and cold plumes through the interior affects the passive upwelling.

6. Boundary Layer Thickness

[20] We now seek a scaling for the boundary layer thickness as a function of Ra and H. It is typically assumed (and is implicit in the discussion of the end-member cases

Table 2. Heat Flow and Temperature Structure Scalings

Value	Scaling	Mean Error (%)
	Top Boundary Layer	
ΔT_{top}	$0.499 + 1.33\ H^{3/4}Ra^{-1/4}$	2.3
Nu_{top}	$0.5H + 0.206\ (Ra - Ra_c)^{0.318}$	5.2
δ_{top}	use $\Delta T_{top}/Nu_{top}$	5.2
	Interior	
T_i	$0.492 + 1.24\ H^{3/4}Ra^{-1/4}$	1.5
$d\mathrm{T}/dz$	$23\ (H/Ra)^{0.52}$	29
	Bottom Boundary Layer	
ΔT_{bot}	$0.514 - 1.13\ H^{3/4}Ra^{-1/4}$	4.6
Nu_{bot}	$-0.5H + 0.206\ (Ra - Ra_c)^{0.318}$	5.4
δ_{bot}	use $\Delta T_{bot}/Nu_{bot}$	10

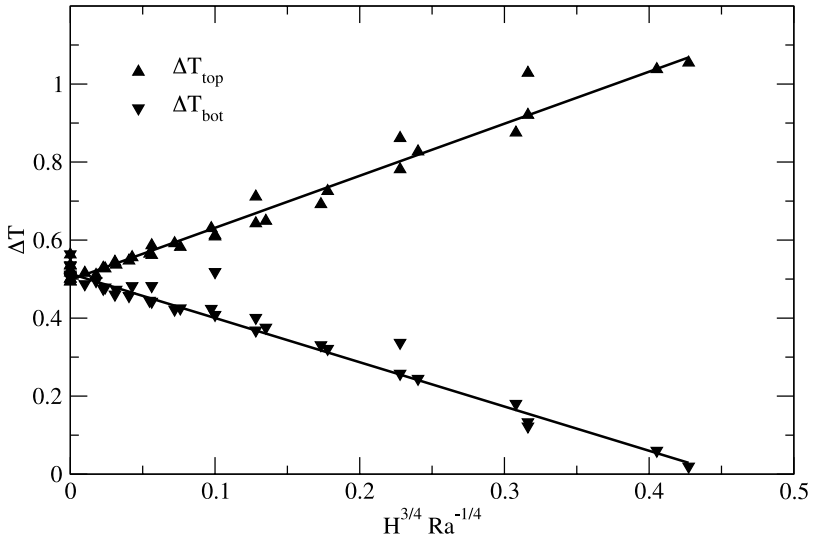

Figure 3. Temperature drop across the upper boundary layer (triangles) and the lower boundary layer (inverted triangles) vs. $H^{3/4}Ra^{-1/4}$. The solid lines are the fitting functions given in (6) and (7) for the upper and lower boundary layers, respectively.

above) that the boundary layer thickness is set by a stability criterion of the form $Ra_b = Ra_c$ [*Howard*, 1966], where the critical Rayleigh number Ra_c is a constant depending on boundary conditions, and the boundary layer Rayleigh number Ra_b is defined as

$$Ra_b = \frac{\rho g \alpha \Delta T_b \delta^3}{\eta \kappa}, \tag{8}$$

where ΔT_b is the temperature drop across the boundary layer and δ is the boundary layer thickness. For bottom-heated cases, ΔT_b is $\Delta T/2$ and the dimensionless boundary layer thickness (δ/D) is seen to scale as $(Ra/Ra_c)^{-1/3}$. In the mixed heating case, ΔT_b is not constant, but the stability criterion predicts the following relationship:

$$\delta = \left(\frac{Ra}{Ra_c}\frac{\Delta T_b}{\Delta T}\right)^{-1/3} \tag{9}$$

which is plotted for the both boundary layers in Figure 5 (mixed heating cases with $Ra = 3 \times 10^5$, 3×10^6, and 3×10^7 have been omitted for clarity but are included in the fits).

[21] The boundary layer thickness for the bottom-heated cases (solid symbols) follows a power-law with Ra_b, and a fit to these for $Ra \geq 10^5$ is shown as a solid line. The best-fit exponent is -0.303, which is significantly lower than the

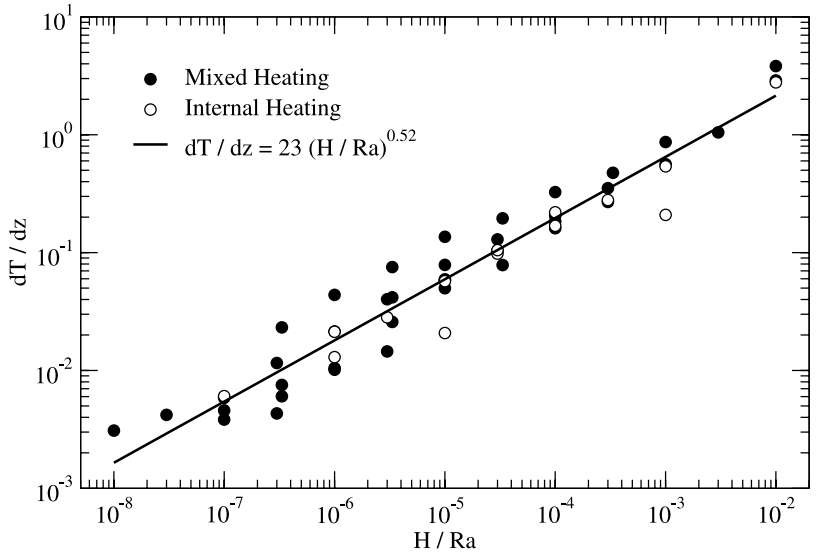

Figure 4. The subadiabatic temperature gradient in the interior of layers with pure internal (open symbols) and mixed heating (solid symbols) vs. H/Ra. The slope is 0.52, very close to the predicted scaling.

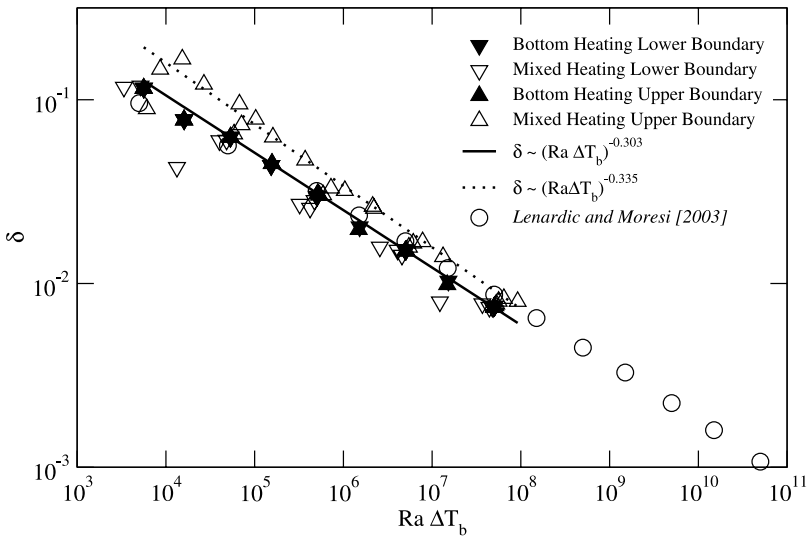

Figure 5. Boundary layer thickness δ vs. boundary layer Rayleigh number $Ra_b = Ra\Delta T_b$. The solid line is a fit to the bottom-heated cases (solid symbols), and the dotted line is a fit to the mixed heating cases in which the bottom boundary Nusselt number is negative (cases with $Ra < 10^5$ have been excluded from the fits). The mixed heating cases with $Ra = 3 \times 10^5$, 3×10^6, and 3×10^7 have been omitted for clarity but are included in the fits. The bottom-heated, 1×1 box calculations of *Lenardic and Moresi* [2003] have been included (circles) for comparison.

predicted $-1/3$. The addition of internal heating, however, results in a divergence in the thicknesses of the boundary layers that is not accounted for by the changing temperature drop across the layer according to (9). Indeed, the response of the boundary layers is opposite to that expected based on the change in the local boundary layer Rayleigh number. The upper boundary layer, which has seen its temperature contrast and Rayleigh number increase, thickens, while the lower boundary layer, which has seen a decrease in the temperature contrast, thins. The departure from the predicted scaling increases with H and decreases with Ra. More specifically, the boundary layer thickness scaling with Ra_b approaches the theoretical $-1/3$ scaling as H increases. A fit (dotted line) to the upper boundary layer thickness for cases with negative bottom Nusselt number (i.e., no bottom boundary layer) results in a best fit exponent of -0.335. Thus the departure of the boundary layer thickness scaling from that predicted by boundary layer stability seems to be due to the presence of flow (plumes) driven by processes at the other boundary.

7. Boundary Heat Flux

[22] Rather than attempt to directly determine the scaling for the boundary layer thicknesses by deriving a new scaling, it is simpler to determine the scaling for the heat flux across the boundaries, and thus to infer the scaling for the boundary layer thicknesses using the relationship: $\Delta T_{bot}/Nu_{bot}$. The advantage in this case is a clear knowledge of the end-member scalings at zero and large H. Since we have the additional constraint that $Nu_{top} = Nu_{bot} + H$, we can fit a single function for the heat flux at both boundaries simultaneously. It is expected that the scaling for the heat flow through the lower boundary changes when Nu_{bot} becomes negative, therefore such cases will not be used to derive the scaling.

[23] According to the previous discussion, the boundary heat flux at $H = 0$ should scale as $Ra^{1/3}$ at large Ra. At low Ra, however, the Nusselt number should equal 1 at the critical Rayleigh number Ra_{c}, and therefore the scaling relationship should have the form:

$$(Nu - 1) \sim (Ra - Ra_c)^{\beta}. \tag{10}$$

These constant offsets are typically ignored under the assumption that they are negligible for the large Rayleigh numbers that apply to planets, however, the effective Rayleigh number in planets is much lower than that implied by the total temperature drop, because the rigid lid (in all cases except Earth) absorbs most of the temperature change without participating in convection [*Solomatov*, 1995]. We will therefore use (10) to fit the heat flow results. The precise value of Ra_{c} is uncertain for mixed heating cases. For bottom-heated cases, Ra_c is 658 from linear stability analysis [*Schubert et al.*, 2001], but it turns out that the fits are quite insensitive to the actual value ($Ra - Ra_{\mathrm{c}}$ is much larger than Nu-1) so this value will be adopted for all fits.

[24] The scaling found from the bottom-heated cases is $(Nu - 1) \sim (Ra - Ra_c)^{0.318}$. The slightly lower than expected exponent is typical of numerical simulations of convection, especially in this range of Ra [*Christensen*, 1989]. At large H, the heat flux should scale linearly with the internal heating as in purely internally heated cases (the coefficient should approach 0.5 in this case as half the heat will escape through the bottom of the layer). Noting that the internal temperature seems to be the sum of the temperature set by the average of the boundaries and the temperature required to remove the internally generated heat (5), let us simply assume that the internally generated heat adds linearly to the heat transported by the temperature difference between the two boundaries (this assumption will be revis-

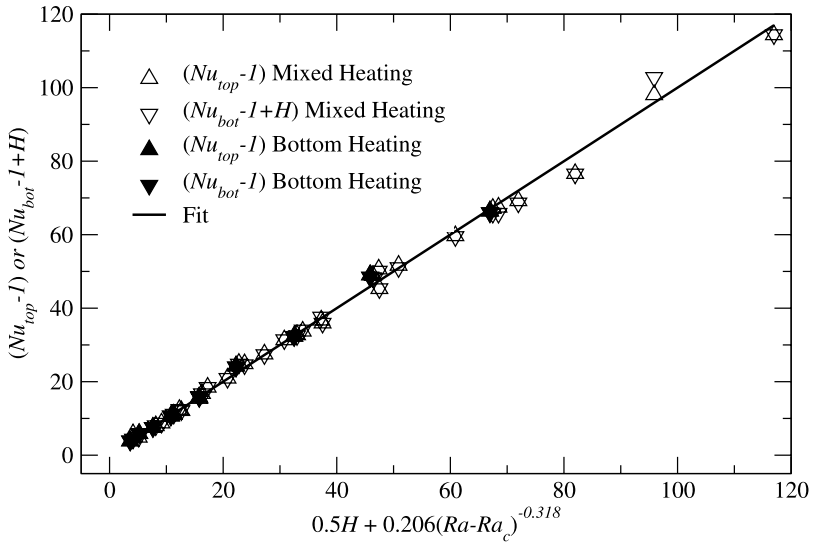

Figure 6. Measured vs. predicted Nusselt numbers at the upper boundary layer (triangles) and lower boundary layer (plus H, inverted triangles) for mixed (open symbols) and bottom heating cases (solid symbols). The solid line shows where the measured values equal those predicted by the model $0.5H + 0.206\ (Ra - Ra_c)^{0.318}$.

ited in the discussion section). We therefore arrive at the following scaling for the heat flux through the boundaries:

$$\begin{aligned}\left(Nu_{top} - 1\right) &= (Nu_{bot} - 1) + H \\ &= 0.5H + 0.206(Ra - Ra_c)^{0.318},\end{aligned} \tag{11}$$

which is shown in Figure 6. The quality of the fit for $Ra \geq 10^5$ is excellent, with average errors of 3% for $(Nu_{top} - 1)$ and $(Nu_{bot} - 1 + H)$. This fit is significantly improved (nearly a factor of two decrease in the average misfit) over a fit which does not include the Nusselt number offset (Nu vs. $Nu - 1$), but the influence of the critical Rayleigh number is small, as found for the bottom-heated cases. The coefficient for H in (11) is not well constrained by fitting (a value of 0.6 ± 0.1 was found) so the expected asymptotic value of 0.5 was adopted, with little change to the quality of the fit. As expected, this relationship does not predict Nu_{bot} well when it is negative.

[25] Returning to boundary layer thickness, the predicted scaling for δ_{top} is now

$$\delta_{top} = \frac{\Delta \mathrm{T}_{top}}{Nu_{top}} = \frac{0.499 + 1.33\ H^{3/4} Ra^{-1/4}}{0.5\ H + 0.206(Ra - Ra_c)^{0.318}}, \tag{12}$$

and the predicted bottom boundary layer thickness is

$$\delta_{bot} = \frac{\Delta \mathrm{T}_{bot}}{Nu_{bot}} = \frac{0.514 - 1.13 H^{3/4} Ra^{-1/4}}{-0.5H + 0.206(Ra - Ra_c)^{0.318}}. \tag{13}$$

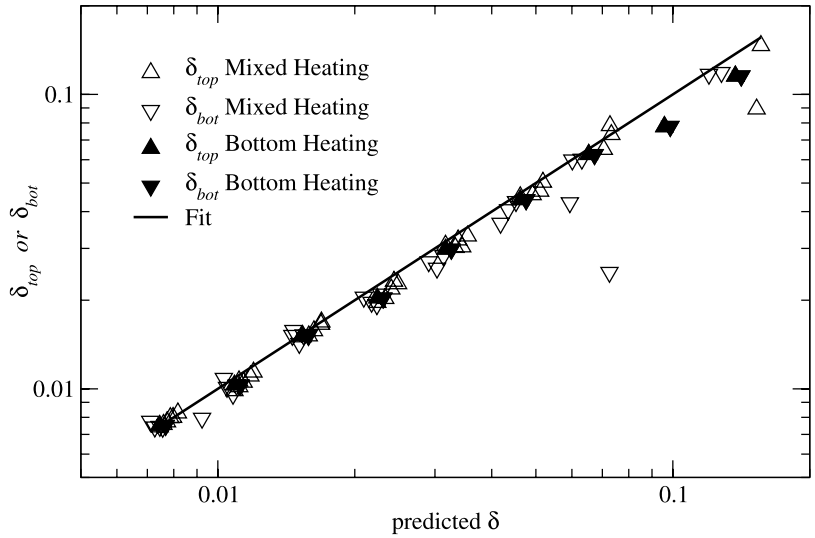

Figure 7. Top and bottom boundary layer thicknesses vs. predicted scalings from (12) and (13), respectively. The solid line shows where the measured values equal the predicted.

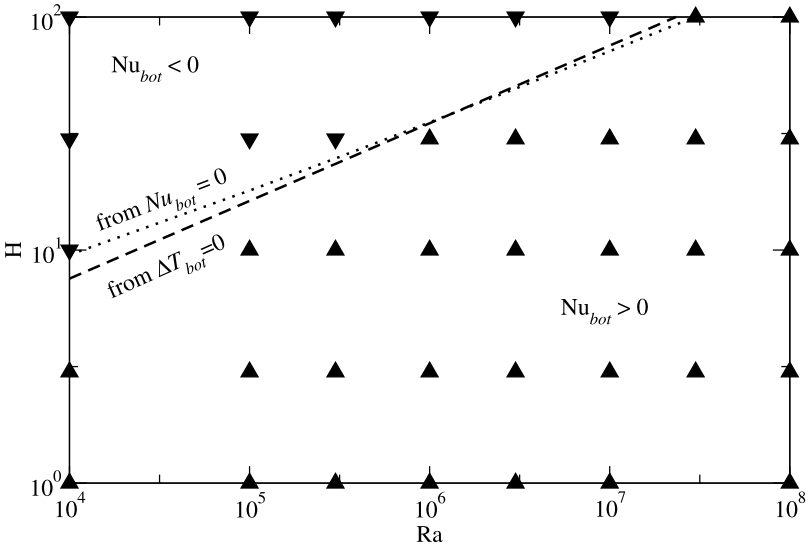

Figure 8. Cases for which Nu_{bot} is positive (triangles) and negative (inverse triangles) as a function of Ra and H. The dashed line is the predicted $Nu_{bot} = 0$ boundary from (7), and the dotted line is derived from (11).

The predicted scaling is shown vs. the measured δ_{top} and δ_{bot} in Figure 7. The fit is quite good, especially for $Ra \geq 10^5$ ($\delta \leq 0.07$), with average errors of 5% for δ_{top} and 10% for δ_{bot} in this range of Ra. This scaling behaves as expected at the extreme values of H. For $H = 0$, δ scales as $Ra^{-0.318}$ and for large H, δ scales as $Ra_H^{-1/4}$. Importantly, one can see from Figure 7 that the trend as H increases (upper boundary layer thickens and lower boundary layer thins) is well predicted for both boundary layers.

[26] The predicted boundary layer thicknesses are not as accurate for the lower boundary layer as for the upper boundary layer, and there are several anomalous points which correspond to extremely weak bottom boundary layers, as Nu_{bot} approaches zero. A curious aspect of layers with mixed heating is that the heat flow through the bottom boundary can become negative if the internal temperature becomes too large. The point at which $Nu_{bot} = 0$ corresponds to a purely internally heated case (though with a different boundary condition). The scaling for ΔT_{bot} predicts that for $H > 0.35Ra^{1/3}$, heat will flow out of the bottom boundary, while the scaling for Nu_{bot} predicts the transition to occur for $H > 2 + 0.412Ra^{0.318}$. Both scalings are essentially indistinguishable and match the numerical solutions as shown in Figure 8.

8. Discussion

[27] Scalings for the heat flow at the boundaries and the temperature structure of convecting layers heated from within and below have been determined (Table 2). The internal temperature and boundary layer temperature drops scale in a way that is similar to the internally heated case, but with an offset that reflects the underlying temperature structure of bottom-heated convection. The surface heat flux scales similarly as a simple addition of the internally generated heat to that transported by the temperature difference between the boundaries. Deriving boundary layer thicknesses from the scalings for heat flux and boundary layer temperature drop provides an excellent fit to the model results.

[28] The mixed heating cases have revealed a previously noted [e.g., *Christensen*, 1989; *Lenardic and Moresi*, 2003] but unexplained departure of bottom-heated convection from the scaling predicted by boundary layer stability theory. It should be emphasized that *Howard*'s [1966] theory was developed as asymptotic for high Ra, and *Lenardic and Moresi* [2003] have shown that the scaling exponent does not converge toward $-1/3$ until Ra exceeds about 10^9 (circles in Figure 5). Indeed, it appears that at low Ra, the Nusselt number (which is inversely proportional to δ) asymptotically approaches a constant value [*Lenardic and Moresi*, 2003, Figure 6], with no dependence on Ra. This asymptotic behavior is removed by fitting to a relationship of the form of (10), revealing that at low Ra, or more precisely low $Ra - Ra_c$, the Nusselt number approaches 1. Thus, while it may be surprising that the effect of finite heat transport in the conduction regime is still noticeable at Rayleigh numbers more than 10^5 times critical, the Nusselt number is only about 30 at $Ra = 10^8$, and the effect of using Nu rather than $Nu - 1$ is to bias any derived scaling toward a lower exponent, an effect that strengthens as the lowest Ra employed decreases.

[29] The observation that the internal temperature increase scales in exactly the same way as for purely internally heated cases and that the heat flux at the surface is simply a sum of internal production and boundary heat transport suggests that there are two parallel heat transport modes operating in the layer. The only way to accomplish this is if there are different processes operating simultaneously in different parts of the boundary layer. That is, there is no single global description of the dynamics of the boundary layer in the mixed heat case. Instead, there must be two different types of dynamics operating over different portions of the boundary.

[30] The implications of this go beyond heat transport in layers with mixed heating. The textbook descriptions of the

behavior of the boundary layer in the bottom and internally heated cases (see discussion above and *Turcotte and Schubert* [2001]) both invoke the instability of a fluid sublayer, which is modified in the case of internal heating to account for the varying internal temperature. However, how can the dynamics of the boundary layer be localized if the same instability mechanism is operating everywhere? Other than having large horizontal gradients in temperature across the domain, which is not observed, there is no way to alter the stability of the sublayer from place to place. The answer is that there are two different instability mechanisms operating in the boundary layer.

[31] For a purely internally heated fluid, it is difficult to imagine what else could control the dynamics of the boundary layer other than the local stability of the sublayer. The theory fits the observations (both laboratory and numerical) very well. In Figure 5, the convergence of the boundary layer thickness to that predicted by stability theory occurs as the system becomes more dominated by internal heating. In the case of bottom-heated convection, however, there is an obvious and, most importantly, localized process that modifies the behavior of the boundary layer: the arrival of plumes from the other boundary. The results presented here suggest that boundary layer stability analysis, though generally considered successful, is not an accurate description of the processes controlling boundary layer thickness at these Rayleigh numbers because the effect of plumes arriving from the other boundary layer is ignored.

[32] By examining a layer with mixed heating that creates asymmetric boundary layers, we see that the arrival of plumes alters the thickness of the boundary layer, for example, the bottom boundary layer in the mixed heating cases, which thins as excess plumes arrive from the upper boundary layer (Figure 5). Only in the case when there is only a single boundary layer (purely internally heated convection) is the boundary able to evolve to the stability limit. Otherwise, the boundary is destabilized by the arrival of plumes that create unstable piles of material between them (as noted by *Labrosse* [2002]). This effect apparently dominates at the Rayleigh numbers investigated here, and is most likely responsible for the consistently low exponents (relative to 1/3) found in the $Nu - Ra$ relationship. This is likely also responsible for the failure of an averaged boundary layer thickening profile to fit the averaged temperature structure [*Parmentier and Sotin*, 2000]. At very high Rayleigh number (the ''hard-turbulent'' regime of *Hansen et al.* [1990]), when the plumes dissipate all of their buoyancy in traversing the interior, their ability to influence the other boundary layer diminishes.

[33] The scalings derived here have several implications for thermal history models. The efficiency of heat transport through the bottom boundary given by (11) depends on two competing terms, one dependent on Ra, and the other dependent on H. As H decreases or Ra increases, the bottom heat flux increases. The long-term evolution of planetary mantles generally sees Ra decrease along with H. Since these two effects offset, the flux out of the underlying layer may be relatively constant over time. If the underlying layer cools off sufficiently rapidly (that is, it has a low heat capacity), Ra decreases while H changes little and the heat flow out of the layer drops. Thus the cooling of the underlying layer is locked to the rate at which H decreases.

[34] The $Nu_{bot} = 0$ condition is an interesting variant on the purely internally heated case. Rather than an insulating boundary condition, which enforces zero heat flux everywhere, the condition is one of zero net flux, a far more realistic description of a passive internal layer. Such cases obey the relationship $H = 0.35Ra^{1/3}$ which implies that the equilibrium temperature drop across an internally heated layer overlying a passive heat sink scales as H^3. Taking the scaling for the non-dimensional temperature drop across a purely internally heated layer $\Delta T_i = 4.91\ \Delta T_H Ra_H^{-1/4}$ [*Turcotte and Schubert*, 2001, equations (6–345)] and setting it equal to the temperature difference between the boundaries in the mixed case (ΔT) leads to the very similar expression $H = 0.15Ra^{1/3}$. Evidently, since the bottom boundary layer isn't actually involved in the convection, the flow is insensitive to the actual boundary condition, and the zero flux condition is appropriate for modeling such systems.

[35] These scalings will be extended to temperature-dependent viscosity fluids and spherical shells in future papers. Temperature-dependent viscosity acts to restrict the temperature drop across the actively convecting region to a few times the rheological temperature scale $\partial \ln(\eta)/\partial T$ [*Yuen and Fleitout*, 1984; *Davaille and Jaupart*, 1993]. Within this layer, the convection is in the small viscosity contrast regime. With a fixed temperature drop, Ra can only adjust by changing the internal temperature which adjusts the viscosity. By balancing the heat flux at the top of the convecting layer with the solution for conduction through the rigid lid, the lid thickness and the temperature structure of the layer may be determined [*Reese et al.*, 2005].

[36] **Acknowledgments.** The author would like to thank R. Kerr and S. Labrosse for thorough and insightful reviews. This work was partially supported by the NASA Astrobiology Institute.

References

Christensen, U. R. (1989), The heat transport by convection rolls with free boundaries at high Rayleigh number, *Geophys. Astrophys. Fluid Dyn.*, *46*, 93–103.

Davaille, A., and C. Jaupart (1993), Transient high-Rayleigh-number thermal convection with large viscosity variations, *J. Fluid Mech.*, *253*, 141–166.

Davies, G. F. (1999), *Dynamic Earth*, Cambridge Univ. Press, London, U.K.

Grasset, O., and E. M. Parmentier (1998), Thermal convection in a volumetrically heated, infinite Prandtl number fluid with strongly temperature-dependent viscosity: Implications for planetary thermal evolution, *J. Geophys. Res.*, *103*(B8), 18,171–18,181.

Grigne, C., S. Labrosse, and P. J. Tackley (2005), Convective heat transfer as a function of wavelength: Implications for the cooling of the Earth, *J. Geophys. Res.*, *110*, B03409, doi:10.1029/2004JB003376.

Hansen, U., D. A. Yuen, and S. E. Kroening (1990), Transition to hard turbulence in thermal convection at infinite Prandtl number, *Phys. Fluids*, *2*, 2157–2163.

Hauck, S. A., and R. J. Phillips (2002), Thermal and crustal evolution of Mars, *J. Geophys. Res.*, *107*(E7), 5052, doi:10.1029/2001JE001801.

Hauck, S. A., A. J. Dombard, R. J. Phillips, and S. C. Solomon (2004), Internal and tectonic evolution of Mercury, *Earth Planet. Sci. Lett.*, *222*(3–4), 713–728.

Howard, L. N. (1966), Convection at high Rayleigh number, in *Proc. 11th Cong. Appl. Mech.*, edited by H. Görtler, pp. 1109–1115, Springer-Verlag, Berlin, Germany.

Labrosse, S. (2002), Hotspots, mantle plumes and core heat loss, *Earth Planet. Sci. Lett.*, *199*(1–2), 147–156.

Lenardic, A., and L. Moresi (2003), Thermal convection below a conducting lid of variable extent: Heat flow scalings and two-dimensional, infinite Prandtl number numerical simulations, *Phys. Fluids*, *15*(2), 455–466.

Parmentier, E. M., and C. Sotin (2000), Three-dimensional numerical experiments on thermal convection in a very viscous fluid: Implications for the

dynamics of a thermal boundary layer at high Rayleigh number, *Phys. Fluids*, *12*(3), 609–617.
Reese, C. C., V. S. Solomatov, and L. N. Moresi (1999), Non-Newtonian stagnant lid convection and magmatic resurfacing on Venus, *Icarus*, *139*, 67–80.
Reese, C. C., V. S. Solomatov, and J. R. Baumgardner (2005), Scaling laws for time-dependent stagnant lid convection in a spherical shell, *Phys. Earth Planet. Inter.*, *149*(3–4), 361–370.
Schubert, G., D. L. Turcotte, and P. Olson (2001), *Mantle Convection in the Earth and Planets*, Cambridge Univ. Press, New York.
Smolarkiewicz, P. K. (1984), A fully multidimensional positive definite advection transport algorithm with small implicit diffusion, *J. Comput. Phys.*, *54*, 325–362.
Solomatov, V. S. (1995), Scaling of temperature- and stress-dependent viscosity convection, *Phys. Fluids*, *7*, 266–274.
Solomatov, V. S., and L. N. Moresi (2000), Scaling of time-dependent stagnant lid convection: Application to small-scale convection on Earth and other terrestrial planets, *J. Geophys. Res.*, *105*(B9), 21,795–21,817.
Sotin, C., and S. Labrosse (1999), Three-dimensional thermal convection in an iso-viscous, infinite Prandtl number fluid heated from within and from below: Applications to the transfer of heat through planetary mantles, *Phys. Earth Planet. Inter.*, *112*(3–4), 171–190.
Tackley, P. J. (1996), Effects of strongly variable viscosity on three-dimensional compressible convection in planetary mantles, *J. Geophys. Res.*, *101*(B2), 3311–3332.
Tozer, D. C. (1967), Towards a theory of thermal convection in the mantle, in *The Earth's Mantle*, edited by T. F. Gaskell, pp. 325–353, Academic Press, London, U.K.
Turcotte, D. L., and G. Schubert (2001), *Geodynamics*, 2nd ed., Cambridge Univ. Press, New York.
Yuen, D. A., and L. Fleitout (1984), Stability of the oceanic lithosphere with variable viscosity: An initial-value approach, *Phys. Earth Planet. Inter.*, *34*, 173–185.

W. B. Moore, Institute of Geophysics and Space Physics and Department of Earth and Space Sciences, University of California, Los Angeles, 3806 Geology Building, Box 951567, Los Angeles, CA 90024-1567, USA. (bmoore@ess.ucla.edu)